Article

Current Biology

A Tandem Amino Acid Residue Motif in Guard Cell SLAC1 Anion Channel of Grasses Allows for the Control of Stomatal Aperture by Nitrate

Graphical Abstract

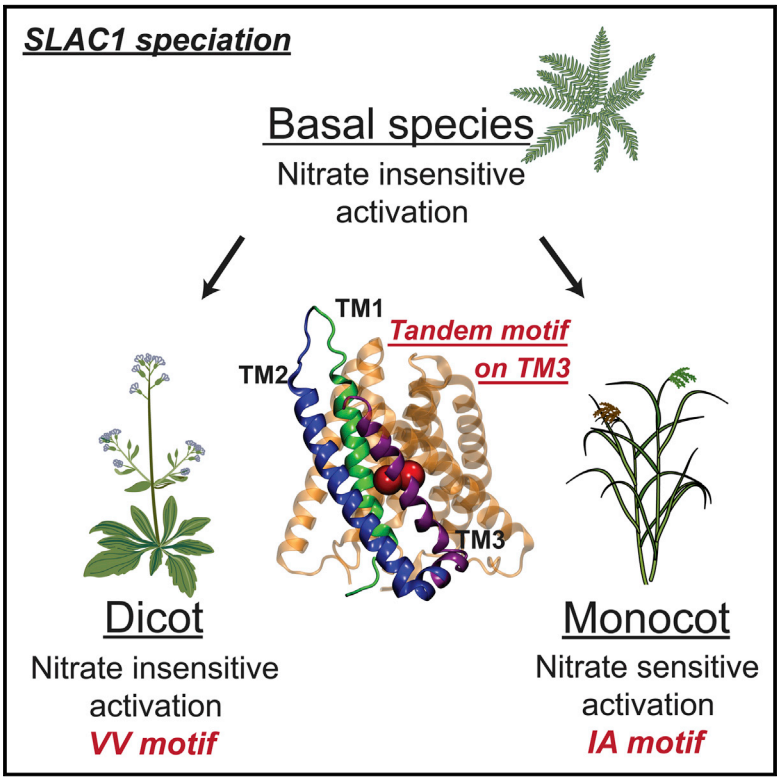

Highlights

- Barley guard cells require nitrate for ABA-triggered fast stomatal closure
- Guard-cell-expressed barley anion channel HvSLAC1 is gated by extracellular nitrate
- Two residues on TMD3 of HvSLAC1 play a crucial role in nitrate-dependent gating
- Monocot SLAC1s developed nitrate-dependent gating after the split from dicots

Authors

Nadine Schäfer, Tobias Maierhofer, Johannes Herrmann, ..., Peter Ache, Dietmar Geiger, Rainer Hedrich

Correspondence

alistair.hetherington@bristol.ac.uk (A.M.H.), geiger@botanik.uni-wuerzburg.de (D.G.), hedrich@botanik.uni-wuerzburg.de (R.H.)

In Brief

Schäfer et al. report that guard cells of the cereal crop barley require nitrate for ABA-induced stomatal closure—a feature accomplished by the guard cell anion channel HvSLAC1. Nitrate-dependent gating of HvSLAC1 and other monocot SLAC1-type anion channels evolved from a TMD3 tandem motif after the split between monocots and dicots.

Schäfer et al., 2018, Current Biology *28*, 1370–1379
May 7, 2018
https://doi.org/10.1016/j.cub.2018.03.027

CellPress

CellPress

Current Biology
Article

A Tandem Amino Acid Residue Motif in Guard Cell SLAC1 Anion Channel of Grasses Allows for the Control of Stomatal Aperture by Nitrate

Nadine Schäfer,[1,5] Tobias Maierhofer,[1,5] Johannes Herrmann,[1,5] Morten Egevang Jørgensen,[1] Christof Lind,[1] Katharina von Meyer,[1] Silke Lautner,[2] Jörg Fromm,[2] Marius Felder,[3] Alistair M. Hetherington,[4,*] Peter Ache,[1] Dietmar Geiger,[1,6,*] and Rainer Hedrich[1,*]

[1]Institute for Molecular Plant Physiology and Biophysics, Julius-von-Sachs-Institute, Biocenter, University of Würzburg, Julius-von-Sachs Platz 2, 97082 Würzburg, Germany

[2]Department of Wood Science, University Hamburg, Leuschnerstrasse 91d, 21031 Hamburg, Germany

[3]Plant Genome and Systems Biology, Helmholtz Center Munich, Ingolstädter Landstrasse 1, 85764 Neuherberg, Germany

[4]School of Biological Sciences, Life Sciences Building, University of Bristol, 24 Tyndall Avenue, Bristol BS8 1TQ, UK

[5]These authors contributed equally

[6]Lead Contact

*Correspondence: alistair.hetherington@bristol.ac.uk (A.M.H.), geiger@botanik.uni-wuerzburg.de (D.G.), hedrich@botanik.uni-wuerzburg.de (R.H.)

https://doi.org/10.1016/j.cub.2018.03.027

SUMMARY

The latest major group of plants to evolve were the grasses. These became important in the mid-Paleogene about 40 million years ago. During evolution, leaf CO_2 uptake and transpirational water loss were optimized by the acquisition of grass-specific stomatal complexes. In contrast to the kidney-shaped guard cells (GCs) typical of the dicots such as *Arabidopsis*, in the grasses and agronomically important cereals, the GCs are dumbbell shaped and are associated with morphologically distinct subsidiary cells (SCs). We studied the molecular basis of GC action in the major cereal crop barley. Upon feeding ABA to xylem sap of an intact barley leaf, stomata closed in a nitrate-dependent manner. This process was initiated by activation of GC SLAC-type anion channel currents. HvSLAC1 expressed in *Xenopus* oocytes gave rise to S-type anion currents that increased several-fold upon stimulation with >3 mM nitrate. We identified a tandem amino acid residue motif that within the SLAC1 channels differs fundamentally between monocots and dicots. When the motif of nitrate-insensitive dicot *Arabidopsis* SLAC1 was replaced by the monocot signature, AtSLAC1 converted into a grass-type like nitrate-sensitive channel. Our work reveals a fundamental difference between monocot and dicot GCs and prompts questions into the selective pressures during evolution that resulted in fundamental changes in the regulation of SLAC1 function.

INTRODUCTION

Guard cell pairs that drive stomatal movement control leaf CO_2 uptake and concomitant transpirational water loss. To survive episodes of drought and excessive heat, stomata have to sense sudden changes in environmental conditions and adjust stomatal aperture accordingly. Based largely on work in the model dicot *Arabidopsis* much is known about the molecular details that underlie stomatal function [1–3]. By way of contrast, in the grasses that are by far the world's most important sources of food, it is surprising that our molecular knowledge concerning guard cell function is still very limited [4–8] (and references therein).

In contrast to the kidney-shaped guard cells typical of the dicots, grass stomata come as pairs of dumbbell-shaped guard cells (GCs) in physical contact with a lateral pair of subsidiary cells (SCs) [4]. In terms of function there, Raschke and Fellows (1971 [9]) found that during stomatal opening in maize K^+ and anions are shuttled from SCs to GCs and when closing they move in the opposite direction. GCs of dicots and monocots respond to the plant hormone ABA that binds to its cytosolic PYR/PYL/RCAR-type receptor [10, 11]. The ABA receptor forms a complex with the PP2C phosphatase ABI1 and SnRK2 kinase OST1 [12]. Binding of ABA to the receptor ABA causes inactivation of ABI1 and release of OST1 from inhibition of the PP2C phosphatase [13]. In turn, the OST1 kinase phosphorylates the GC anion channel SLAC1, causing it to open [14, 15]. The resulting release of anions depolarizes the plasma membrane, and the change in voltage activates the GORK1 channel resulting in K^+ efflux, which is followed by the loss of water and resulting stomatal closure [1, 16].

Potassium and chloride represent the dominant ions in dicot and monocot GCs. In the dicot model plant *Arabidopsis*, the SLAC1 channel is permeable to chloride. When expressed in the heterologous expression system of *Xenopus* oocytes, *Arabidopsis* SLAC1 is active in chloride-based media [14]. In contrast to SLAC1, its homologs SLAH2 and 3 require nitrate at the external mouth of the anion channel to gate open in oocyte and GC systems [17, 18]. In order to gain insights into how cereal GCs function, we analyzed the transcript profile of barley GCs and SCs. We identified HvSLAC1 together with the major components of GC ABA signaling. Strikingly, in barley SLAC1 and in marked contrast to *Arabidopsis* SLAC1, we identified a distinct tandem amino acid motif, responsible for nitrate activation.

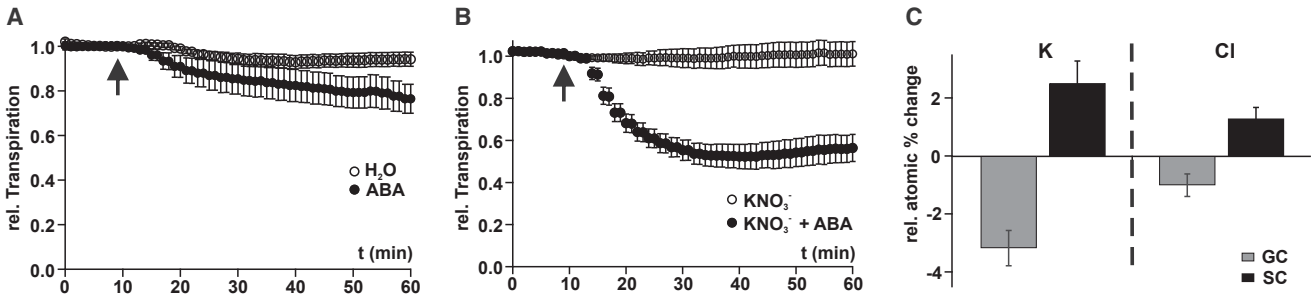

Figure 1. ABA-Induced Stomatal Closure Requires NO_3^-

Barley stomatal movement measured by infrared gas exchange. Barley stomata were opened in the light (400 μE) at ambient CO_2 (400 ppm).

(A) Excised leaves were supplied with water and ABA via the transpiration stream. Note, stomatal closure in the presence of ABA was remarkably slow and largely incomplete.

(B) Leaves were pre-incubated with 5 mM nitrate. Under this condition, leaves started to close their stomata 5 min after ABA application. This process was largely completed within 10 min and finished in less than 15 min. Data were normalized to their open value 10 min before the application of ABA (indicated by the arrow). $n \geq 5$ means ± SE.

(C) EDX analysis of barley stomatal complexes. The respective changes in K (left) and Cl contents (right) are shown after the transition from open to closed stomata in guard cells (GC) and subsidiary cells (SC). During stomatal opening, potassium and chloride ions shuttle from SCs to GCs, while ions move in the opposite direction when stomata close. n = 11, means ± SE.

RESULTS

ABA-Dependent Stomatal Closure in Barley Requires Extracellular Nitrate

Surprisingly, studies aimed at understanding the molecular basis of stomatal movements in barley, a major cereal grass crop, are somewhat limited [4, 5]. To address this issue, we first investigated stomatal function in the intact barley leaf using infrared gas analyzer (IRGA)-based measurements of stomatal conductance. We focused on *Hordeum vulgare* line Barke, because genome information is available, and it represents one of the most popular brewing barley varieties worldwide.

From work in *Arabidopsis*, it is known that ABA triggers stomatal closure following binding to cytosolic receptors of the PYR/PYL family and the subsequent induction of a signaling pathway that ultimately activates SLAC/SLAH anion channels [14, 15, 17, 19, 20]. To investigate the response of barley stomata to ABA, we fed 25 μM ABA (a concentration sufficient to close barley stomata [5]) via the leaf petiole. When the petiole was supplied with ABA in water, stomatal closure was delayed and incomplete (Figure 1A). This is in marked contrast to the prompt closure observed in the dicot *Arabidopsis* [21] but is similar to the response observed in the monocot date palm [21]. However, the most striking result to emerge from this experiment was that timely and significant ABA-induced stomatal closure could be elicited by the addition of nitrate (5 mM KNO_3^-) to the feeding medium (Figure 1B). This results clearly shows that in barley the full stomatal response to ABA requires the presence of nitrate.

Stomatal Closure in Barley Involves Inverse Fluxes of K^+ and Cl^- between Guard and SCs

Having identified a requirement for nitrate in ABA-induced closure we next investigated the requirement for K^+ and Cl^-. Given that early studies in maize provided initial evidence for K^+ and chloride shuttling between GCs and SCs [9, 22], we used Energy dispersive X-ray (EDX) analysis to determine the content of these elements in guard and SCs. Figure 1C shows that GCs from closed stomata contained less K and Cl than open ones. SCs, however, exhibited the inverse relationship with relatively higher levels of K and Cl associated with closed stomata (Figure 1C). These data confirm older work in maize [9, 22] but leave open the question of why there is a requirement for nitrate for the closure of barley stomata. In summary, in barley just as in *Arabidopsis*, K^+ and Cl^- represent major ionic components of the GC osmotic motor that drives stomatal movement. The fact that the changes in K^+ are larger than those of Cl^- indicate that, besides Cl^-, additional anions such as nitrate or malate must be involved. In this context, it should be mentioned that in barley epidermal cells Cl^- and NO_3^- might provide the total negative solute charge [23].

Using Transcriptomics to Investigate ABA-Induced Stomatal Closure in Barley

To investigate the molecular machinery responsible for bringing about stomatal closure in barley and in particular the ion fluxes between guard and SCs, we employed a transcriptomic approach. We isolated three experimental preparations: (1) intact leaves (L), (2) lower epidermis with intact stomatal complexes (GCSCs), and (3) leaves without upper and lower epidermis and thus without GC complexes (LwoGC). We employed a bioinformatic approach to identify differentially expressed genes (DEG) in GC complexes (for full DEG list, see Table S1). Because GCs, in contrast to mesophyll cells, contain a reduced number of chloroplasts and epidermal pavement cells have no chloroplasts, we initially compared photosynthesis (PS)-related transcripts. As expected, we found genes associated with PS electron transport and CO_2 fixation underrepresented in the GCSC samples (Table S1, filtered by MapMan category 1). When analyzing RNA sequencing (RNA-seq) data, it did not come as a surprise that we found DEGs related to GC function and ABA signaling.

We next investigated genes involved in ion transport. In the ion channel fraction GC-specific anion channels of the *SLAC/SLAH* type and Shaker-like potassium channels of the *KAT* and

GORK/SKOR type were identified (Table S2). This expression pattern underpins the notion that the grass-type stomata from barley harbor the GC major H^+, K^+, and Cl^- transporting entities represented by *AHA1* and *KAT1* for stomatal opening [24] and *SLAC1* and *GORK* for closure ([1] for review). Among the ABA-dependent transcripts, pronounced GC expression of orthologs to the *PYR/PYL* ABA receptor family, *PP2C* phosphatases *ABI1* and *2*, and *SnRK2* kinases of the *OST1* type were found. Based on 5 *HvOST1*-like sequences, we generated a phylogenetic tree and identified *HvOST1.1*, *1.2*, and *1.3* most closely related to the *Arabidopsis OST1* (Figure S1A).

To validate expression of the GC ion channels and components of the ABA signaling pathway suggested by the RNA-seq data, we performed qPCR analysis. We sampled leaves (L) and epidermal peels containing both GCs and SCs (GCSCs) and preparations in which the SCs were selectively disrupted using the blender method [25]. The latter preparation represented a fraction highly enriched in GCs (Figure S1B). As in *Arabidopsis* GC databases obtained using a related experimental approach [25], we found transcripts of *ABI1*, *SLAC1*, and *OST1*.1 expressed in an almost GC-specific manner. In contrast, *OST1.3* expression was found distributed equally among samples. Among the GC-expressed *SnRK2* genes, HvOST1.1 shows the closest phylogenetic relationship to the *Arabidopsis* OST1 kinase with 80.5% identical residues (Figure S1A). The HvOST1.1 sequence harbors all known functional domains of OST1-like, ABA-dependent SnRK2 kinases, including the DI domain/SnRK2 box and the DII domain/ABA-Box [12, 26–28]. On these grounds, HvOST1.1 very likely represents the SLAC1 activating ABA kinase in barley. In *Arabidopsis* GCs SLAH3 operates a nitrate-activated anion channel conducting nitrate and chloride [17]. In barley, however, *SLAH3.1* was found expressed in leaves, but not in the GCSC and GC samples (Figure S1B).

Barley HvSLAC1 Is under the Control of Nitrate and OST1 /ABI1 Pair

McAdam et al., 2016 [29] and Lind et al., 2015 [30] showed that SnRK2 kinases (OST1s) are strictly conserved during evolution. All OST1 kinases derived from different evolutionary distinct plant species so far tested are capable of activating *Arabidopsis* SLAC1. In addition, AtOST1 is capable of activating SLAC1 isoforms from other monocot species, such as PdSLAC1 from date palm [21] or OsSLAC1 from rice [8]. Thus, to understand the molecular basis of nitrate dependency of stomatal closure in barley, we expressed HvSLAC1 alone and together with AtOST1 in *Xenopus* oocytes and studied its anion channel properties. In the absence of the SnRK2 kinase, no currents were recorded and, even in the presence of the ABA-induced kinase AtOST1 and 30 mM chloride-based extracellular media, macroscopic S-type anion currents could be recorded only at strongly depolarized membrane potentials (Figure 2A). Upon addition of 30 mM nitrate, however, pronounced S-type anion currents were observed (Figure 2A). While the *Arabidopsis* OST1 wild-type (WT) kinase was capable of activating HvSLAC1 in nitrate-based solutions, the kinase dead mutant AtOST1 D140A could not perform this function (Figures 2B and 2C). This indicates that phosphorylation of HvSLAC1 is strictly required for anion channel activation (cf. [14].). Besides the calcium-independent SLAC1 kinase OST1, calcium-dependent kinases of the CPK and CIPK/CBL type can phosphorylate and gate open AtSLAC1 ([31]). As a representative of the latter kinases category, we selected CPK6 for oocyte co-expression experiments with HvSLAC1. As with OST1, CKP6 activated the barely S-type channel to the same extent as AtSLAC1 (Figures 2A and S2A [19, 32]).

In contrast to the grass SLAC1, *Arabidopsis* SLAC1 does not require the presence of extracellular nitrate for activation (Figure S2A, cf. [18]). Interestingly, the ABA phosphatase ABI1 in *Arabidopsis* GC inhibits the response to nitrate [33] and negatively regulates AtOST1 and AtSLAC1 activity [14, 15, 19, 31]. Upon co-expression of HvSLAC1 and AtOST1 with ABI1, we found that HvSLAC1-mediated anion currents were strongly reduced (Figures 2B and 2C). These findings indicate that fast ABA signaling is conserved between GCs of the dicot *Arabidopsis* and monocot grass *Hordeum vulgare*.

The *Arabidopsis* AtSLAC1 does not require extracellular nitrate for activation (Figure S2A) but has a strong permeably preference for nitrate over chloride [14]. The HvSLAC1 P_{NO3}/P_{Cl} calculated permeability ratio of 6.4 ± 0.8 indicates that the dicot and monocot GC anion channel would preferentially conduct nitrate when present in GCs at osmotically relevant quantities (Figure S2B). Is the nitrate sensitivity a unique feature of HvSLAC1 or is it found in other cereals, too? To answer this question, we expressed rice SLAC1 (OsSLAC1) in oocytes (cf. [8].). The results in Figures S2A and S2C show that the rice S-type anion channel shared its selectivity and nitrate-dependent features with the Hordeum SLAC1 anion channel. In this context, it should be noted that we recently showed, in the monocot *Phoenix dactylifera* (date palm), that PdSLAC1 is also nitrate activated [21]. Besides nitrate, other physiological relevant anions such as phosphate, sulfate, malate, or chloride were not capable of activating HvSLAC1-derived anion currents (Figure S2D) or to shift its relative P_O to negative (physiological) membrane potentials (Figure S2E).

To find out whether nitrate activation is a property of monocot SLAC1, we compared the Brassicaceaen AtSLAC1 with a dicot ortholog from tomato and tobacco—two Solanaceae crop species. These dicot SLAC1s behave more similarly to the nitrate insensitive AtSLAC1 than to nitrate-activated monocot SLAC1s (Figure 2D).

Extracellular Nitrate Primes HvSLAC1 to Release Chloride

To study the biophysical properties of nitrate-activated HvSLAC1 in more detail, we co-expressed the anion channel with AtCPK6 [2, 19, 32] and determined current densities and the relative open probability as a function of the external nitrate concentration (Figures 3A and 3B). When exposed to increasing external nitrate concentrations, the peak efflux currents and the relative open probability shifted toward negative membrane potentials and thereby increased the plasma membrane anion conductance (Figures 3A and 3B). In contrast, similar experiments with increasing external chloride applications revealed that in the physiological membrane potential range (negative from −100 mV), anion release currents are absent irrespective of the external Cl^- concentration (Figures 3C and 3D). While 100 mM nitrate shifted the HvSLAC1 half-maximal open probability ($V_{1/2}$) to −120 mV (Figure 3B), $V_{1/2}$ in 100 mM chloride

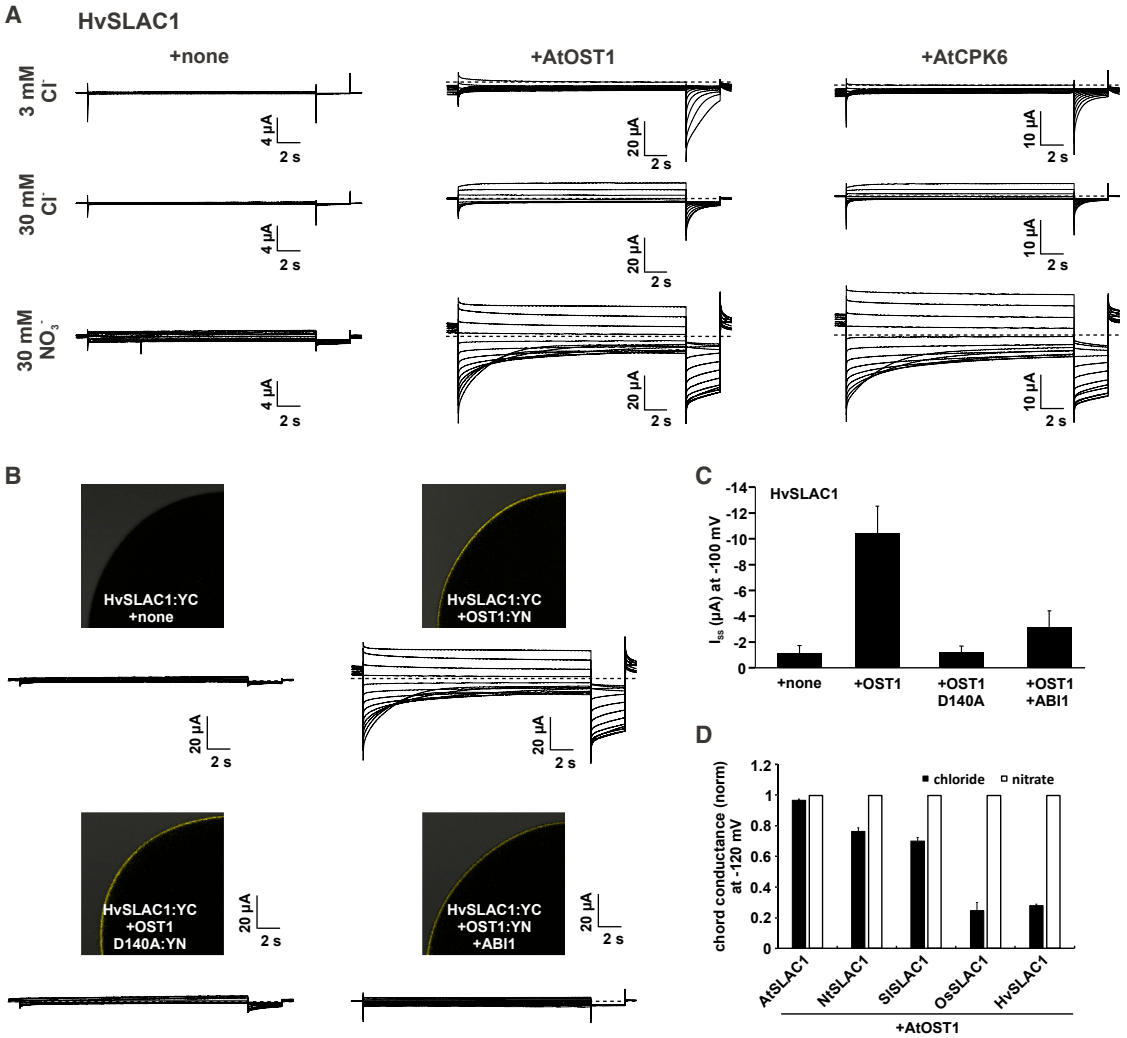

Figure 2. Nitrate-Dependent Activation of HvSLAC1

(A) Whole-oocyte currents of *Xenopus* oocytes expressing HvSLAC1 alone or co-expressing either AtOST1 or AtCPK6 were measured in response to the standard voltage protocol. Currents were recorded in standard buffers containing either 3 mM chloride, 30 mM chloride, or 30 mM nitrate. Representative cells of 2 independent experiments with n = 3 oocytes are shown.

(B) Whole-oocyte currents of oocytes expressing HvSLAC1 equipped with the C-terminal half of YFP (HvSLAC1:YC) either expressed alone or together with WT OST1, OST1 D140A, or WT OST1 and ABI1. Both OST1 versions were fused to the N-terminal half of YFP (OST1:YN, OST1 D140A:YN). Currents were recorded in nitrate-based buffers (30 mM). Representative cells are shown. Co-expression of HvSLAC1 and OST1 or OST1 D140A was confirmed by detection of YFP fluorescence. Quarter of representative oocytes of 2 independent experiments with n = 4 oocytes are shown.

(C) Statistical analysis of the steady-state currents at −100 mV derived from the experiment described in (B) (n = 4 experiments, mean ± SD).

(D) Chord conductance recorded at a membrane potential of −120 mV of oocytes co-expressing AtOST1 with SLAC1 from different plant species indicated in the figure. Chord conductance was calculated from instantaneous currents recorded in chloride- or nitrate-based buffers (100 mM). Chord conductance in nitrate was set to 1 ($n \geq 4$ from 2 independent experiments, mean ± SD).

See also Figure S2.

remained at depolarized membrane potentials of −20 mV (Figure 3D). When plotting $V_{1/2}$ as a function of the external nitrate concentration, the resulting saturation curve could be described with a Michaelis-Menten equation (Figure 3E) resulting in a $K_{0.5}$ value of 10.9 ± 3.8 mM nitrate. Thus, physiological [NO_3^-] concentration of 10–70 mM found in the xylem sap of barley leaves [34, 35] will activate HvSLAC1 anion channel. This set of experiments shows not only that HvSLAC1 conducts nitrate (Figures 3A, 3B, and S2B), but also that nitrate is required to gate the barley GC channel open.

Nitrate-dependent gating is a known feature of SLAH2 and SLAH3 branch of the *Arabidopsis* SLAC/SLAH anion channel family, but not of its founding member AtSLAC1 (see above and cf. [17, 18]; Figure S2A). While AtSLAH2 is strictly nitrate selective, AtSLAH3 also conducts chloride when primed with extracellular nitrate [17, 18]. To further examine the nature of the nitrate dependency of HvSLAC1 and to substantiate that HvSLAC1 conducts chloride in the presence of its gating ligand nitrate, the anion channel was challenged by different chloride to nitrate ratios. Anion currents recorded in the presence of 3 mM

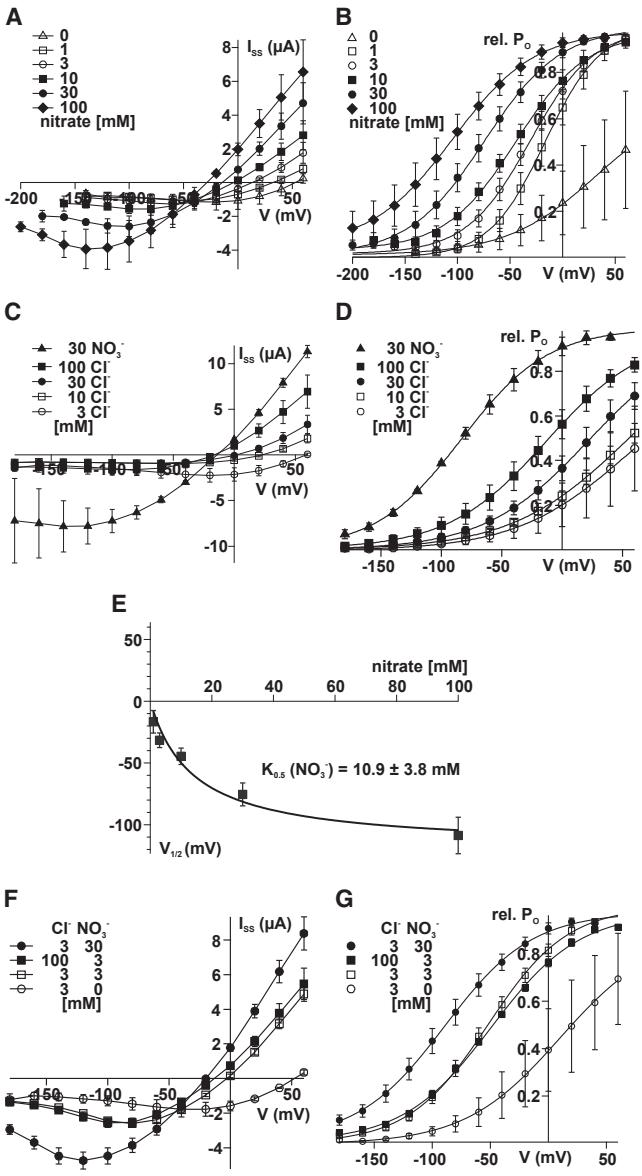

Figure 3. Nitrate Activates HvSLAC1 by Shifting Its Relative Open Probability to Hyperpolarized Voltages

(A) Nitrate dependence of steady-state currents (I_{SS}) of oocytes co-expressing HvSLAC1 and AtCPK6 are plotted as a function of the applied membrane potential (n = 4 from 2 independent experiments, mean ± SD).

(B) The relative open probability (relative P_O) measured in different NO_3^- concentrations of HvSLAC1/AtCPK6-expressing oocytes was plotted against the membrane potential. Data points were fitted with a single Boltzmann equation (solid lines, n = 4 from 2 independent experiments, mean ± SD).

(C) Steady-state currents (I_{SS}) of oocytes co-expressing HvSLAC1 and AtCPK6 recorded in the presence of different external chloride concentrations or 30 mM nitrate (n = 4 from 2 independent experiments, mean ± SD).

(D) The relative open probability (relative P_O) of HvSLAC1 in the presence of different Cl^- concentrations or 30 mM NO_3^- was plotted against the membrane potential. Data points were fitted with a single Boltzmann equation (solid lines, n = 4 from 2 independent experiments, mean ± SD).

(E) The half-maximal P_O ($V_{1/2}$) calculated from the data in (B) was plotted against the nitrate concentration. A Michaelis-Menten equation was used to calculate a $K_{0.5}$ of 10.9 mM NO_3^- (n = 4, mean ± SD).

(F) Steady-state currents of HvSLAC1 and AtCPK6 co-expressing oocytes in the presence of different Cl^-/NO_3^--ratios were plotted against the applied voltage (n = 4 from 2 independent experiments, mean ± SD).

(G) The relative open probability (relative P_O) of HvSLAC1 in different Cl^-/NO_3^--ratios was plotted against the membrane potential.

Data points were fitted with a single Boltzmann equation (solid lines, n = 4 experiments, mean ± SD). See also Figure S2.

extracellular chloride were very weak and reversed at +50 mV (Figure 3F). In contrast, addition of 3 mM nitrate enhanced the steady-state currents and shifted the reversal potential to 0 mV (Figure 3F). When the chloride concentration was further increased to 100 mM in the presence of 3 mM nitrate, the reversal potential of HvSLAC1-mediated anion currents shifted to more negative membrane potentials without anion release currents and relative open probability being influenced by chloride (Figures 3F and 3G). To further investigate the chloride conductance of HvSLAC1 when primed with extracellular nitrate, we monitored the reversal potential of HvSLAC1 AtCPK6-expressing oocytes. Upon addition of 3 mM nitrate to a 3-mM-chloride-containing bath solution, the reversal potential dropped by 56 mV and shifted to even more negative membrane potentials when the chloride concentration was increased to 100 mM (Figures S2F and S2G). This behavior and those to varying Cl^- to NO_3^- rations (Figures 3F and 3G) indicate that HvSLAC1, when pre-activated by nitrate, conducts both nitrate and chloride. In contrast to the nitrate sensitive monocot S-type anion channels, AtSLAC1 reversal potential shifts appeared less nitrate but more chloride sensitive (Figures S2F and S2G). In contrast to AtSLAC1, OsSLAC1, and HvSLAC1, the reversal potential of the nitrate-selective AtSLAH2 was sensitive to nitrate only but not to chloride (Figures S2F and S2G). Taken together, the electrical properties of the monocot anion channels are reminiscent of the nitrate-gated, chloride, and nitrate-permeable AtSLAH3 anion channel rather than of the nitrate-independent dicot AtSLAC1.

SLAC1 Grass-type Tandem Amino Acid Motif on TMD3 Is Key for Nitrate Priming

3D homology modeling of AtSLAC1 and AtSLAH2 to the crystal structure obtained with the bacterial homolog HiTehA in combination with site-directed mutagenesis showed associated residues of Trans-Membrane Domain TMD3 as part of the pore forming entity [18, 36]. To find the nitrate site in barley SLAC1, we compared TMD3 of monocot and dicot SLAC1-type channels (Figures 4A and S3). Monocot and dicot SLAC1s could be well distinguished by two residues close to Val272 and Val273 of AtSLAC1. We found dicot SLAC1s to either carry two valine residues such as AtSLAC1 (V272 and V273) or an IV pair in Solanaceaen species. Monocots including barley HvSLAC1 and date palm PdSLAC1 at the related positions harbor an isoleucine and alanine side chain (Figures 4A and S3) similar to the nitrate-activated SLAH2/3 anion channels that possess either the IA or an IS motif (Figure S3). Given that the amino acid sequence on TMD3 clearly distinguishes monocot from dicot SLACs, these residues seem to represent a specific signature. Thus, we tested whether this TMD3 tandem motif between both monocot and dicot representative SLACs is essential for nitrate dependency. Therefore, we replaced just the VV motif in AtSLAC1 by IA and

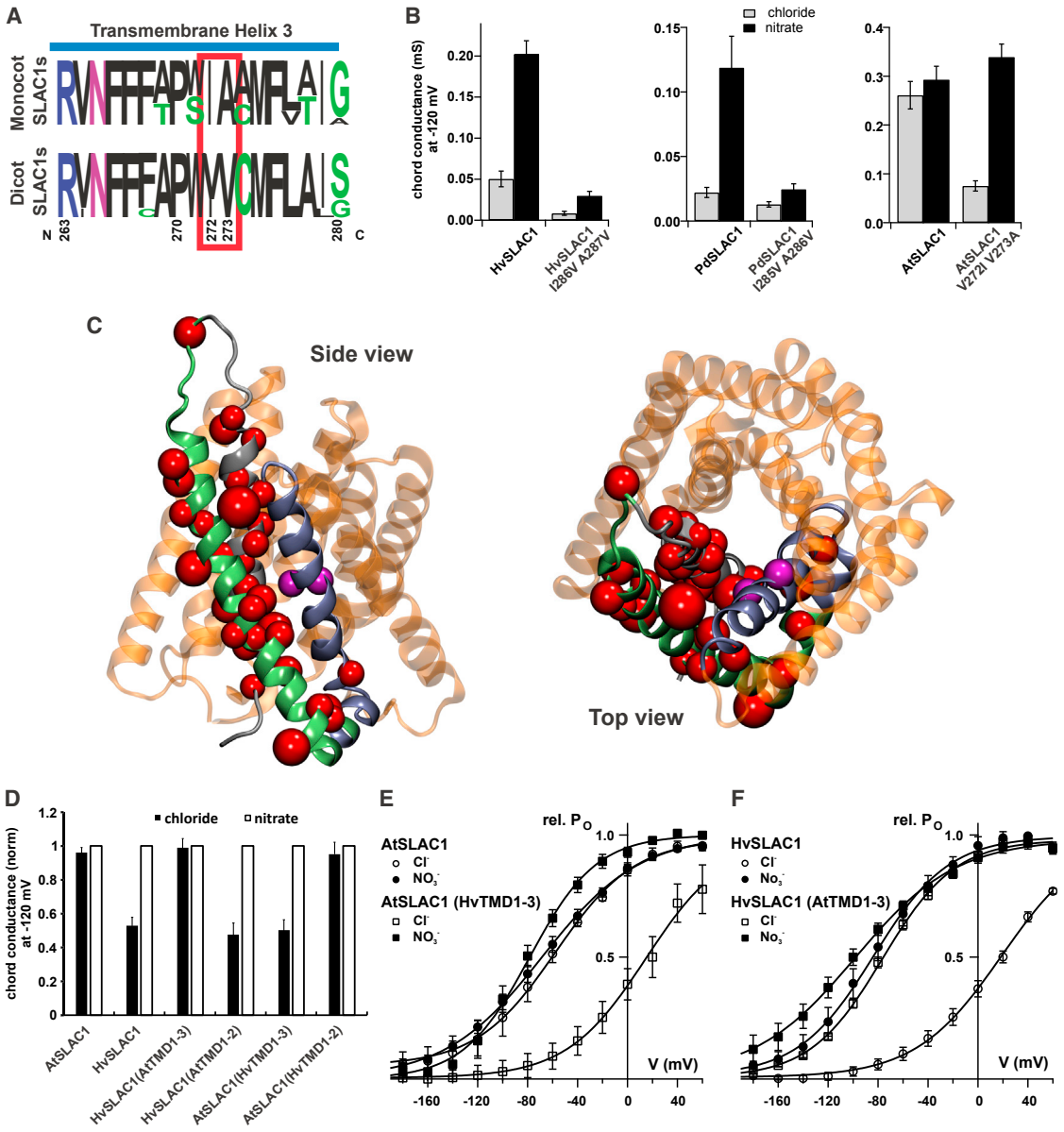

Figure 4. IA-Motif on TMD3 Coevolved with Residues on TMD1 and 2 to Provide Monocot SLAC1 Anion Channels with a Nitrate-Depending Gating Mechanism

(A) Frequency logos of transmembrane three (TMD3) from SLAC1 anion channels of different monocot or dicot species. The respective sequence alignment is shown in Figure S3. The most prominent difference (IA motif in monocots versus VV/IV motif in dicots) is marked with a red box.

(B) Chord conductance at −120 mV of AtSLAC1 WT and AtSLACa1 V272I V273A compared to HvSLAC1 WT and HvSLAC1 I286V A287V or PdSLAC1 WT and PdSLAC1 I285V A286V. All channels and mutants thereof were co-expressed with CPK6. Currents were recorded in nitrate- or chloride-based buffers. (n = 4 from 2 independent experiments, mean ± SD). Note, the phenotypes of HvSLAC1 and AtSLAC1 anion channels were highly reproducible showing nitrate-independent gating properties of AtSLAC1 and nitrate-dependent gating of HvSLAC1 expressing oocytes. In contrast, with the mutant AtSLAC1 V272I V273A we observed a conditional phenotype strongly dependent on the investigated oocyte batch. In 30% of the tested oocyte batches, the mutations in the selectivity signature converted AtSLAC1 into a HvSLAC1-type nitrate-dependent anion channel (these data are shown in this study), whereas the remaining oocyte batches revealed a AtSLAC1 WT behavior.

(C) Evolutionary coupling analysis. The top 50 amino acid residues (see also Table S3) that showed evolutionary coupling to AtSLAC1-V272 and V273 (purple spheres) were highlighted in red on previously generated homology models [18, 36] using VMD [37]. Note, some of the highlighted residues co-evolved with both V272 and V273. The sphere size of co-evolved residues does not relate to the evolutionary coupling strength but reflects the side chain size. TMD1 is depicted in light gray, TMD2 in green, and TMD3 in dark gray. The remaining TMDs are shown in transparent orange.

(D) Chord conductance of oocytes co-expressing AtCPK6 with AtSLAC1, HvSLAC1, or one of the indicated chimeras. Currents were recorded in nitrate or chloride-based buffers. Chord conductance for nitrate was set to 1 (n = 4 from 2 independent experiments, mean ± SD). See also Figure S4B.

(E and F) Relative open probability (relative P_O) of (E) AtSLAC1 and the chimera AtSLAC1(HvTMD1–3) or (F) HvSLAC1 and HvSLAC1(AtTMD1–3) in the presence of 30 mM chloride or nitrate (n = 4 from 2 independent experiments, mean ± SD).

See also Figures S3 and S4 as well as Tables S3 and S4.

the IA motif in Hv/PdSLAC1 by the dicot VV motif. The resulting *Arabidopsis* mutant AtSLAC1 V272I V273A displayed nitrate-induced anion currents just like HvSLAC1 and PdSLAC1 WT (Figure 4B). Note, this behavior appeared only in 30% of the tested oocyte batches (this conditional phenotype is shown in Figure 4B), whereas the remaining oocyte batches revealed a AtSLAC1 WT behavior. Thus, the introduction of the monocot IA motif in TMD3 of AtSLAC1 is essential and sufficient to provide for the nitrate dependency. However, when the monocot SLACs were equipped with the dicot VV signature, the resulting mutants with barley (HvSLAC1 I286V A287V) and date palm anion channel (PdSLAC1 I285V A286V) appeared severely impaired even in nitrate-based buffers (Figure 4B) indicating that in monocots additional structural moieties shape the permeation pathway. The fact that the HvSLAC1 I286V A287V and the PdSLAC1 I285V A286V mutant did not carry macroscopic anion currents and that AtSLAC1 V272I V273A displayed a conditional phenotype only indicates that we have identified a critical position within the selectivity filter in the anion channels' pore that might result in a meta-stable structure in the mutant AtSLAC1 V272I V273A. Thus, it is tempting to speculate that for proper anion discrimination additional residues are involved.

To find a molecular explanation to this discrepancy in monocot-dicot pore residue exchange, we thus asked which channel sites co-evolved with the TMD3 signature. Using a bioinformatics co-evolution pipeline (http://evfold.org/evfold-web/evfold.do), we identified residues in AtSLAC1 that co-evolved with the signature motif. Interestingly, the 50 highest scoring hits of co-evolved residues were found exclusively on TMD1–3 but not on other parts of the SLAC1 protein (Figure 4C; Table S3). To test whether TMD1–3 including the remarkable difference in TMD3 between monocot and dicot SLAC1 representatives is essential and sufficient to provide for the monocot nitrate dependency and dicot nitrate independency, we exchanged either only TMD1 and 2 or TMD1, 2, and 3 between AtSLAC1 and HvSLAC1. The resulting chimeras were named AtSLAC1(HvTMD1–2) where AtSLAC1 carries TMD1 and 2 from HvSLAC1, AtSLAC1(HvTMD1–3) where AtSLAC1 carries TMD1–3 from HvSLAC1 and vice versa. When comparing WT SLAC1 channels with the chimeras where only TMD1 and 2 was replaced, we could not document any change in their chord conductance (Figure 4D). Only when TMDs 1–3 were exchanged, the nitrate dependency of HvSLAC1 could be transferred to AtSLAC1, while HvSLAC1 lost its nitrate dependency when equipped with TMD1–3 of AtSLAC1 (Figure 4D). The comparison of relative open probabilities between AtSLAC1 WT and AtSLAC1(HvTMD1–3) demonstrates that the activation of the chimera is based on a nitrate-dependent shift of its relative P_O to negative membrane potentials just like with monocot HvSLAC1 WT (Figures 4E and 4F). On the contrary, the chimera HvSLAC1(AtTMD1–3) appeared open even in the absence of nitrate, just like dicot AtSLAC1 WT (Figures 4E and 4F). Thus, the TMD3 IA signature from monocots is required and sufficient to convert the dicot SLAC1 from *Arabidopsis* into a nitrate-gated monocot grass SLAC1 anion channel (Figure 4B). In contrast, monocot SLAC1s require the VV motif and in addition backbone residues situated on TMD1 and 2 to be converted in a nitrate-insensitive anion channel (Figures 4D–4F).

DISCUSSION

One of the most striking results to emerge from the experiments described in this paper is that the rates of stomatal opening and closure in barley are much faster than in *Arabidopsis* (cf. [38].). In the absence of other compensatory factors, this is likely to confer a selective advantage on barely in comparison with *Arabidopsis*. The ability to rapidly adjust stomatal aperture to suit the prevailing environmental conditions is likely to allow barley enhanced control over transpiration, xylem-based nutrient delivery, and PS that will likely play out in terms of increased competitiveness ([4, 39] and references therein).

In seeking a mechanistic explanation for the ability of barley stomata to open and close rapidly, we focused first on the flux of the major osmotically active cations and anions. Our results suggest that barley has evolved a stomatal system in which the guard and SCs behave as a functional unit [4, 38]. For example, during closure, while there is loss of K^+, Cl^- (Figure 1C), and very likely NO_3^- too from the GC, it accumulates in the SCs. In this sense, the SCs have evolved to play a role as reservoirs or cisterns of osmotically active ions. In grasses stomata move faster than those of dicots because GCs and SCs actively regulate turgor and volume in an inverse manner [4, 9]. This way SCs operate as a source of osmotica that is used by GCs when they swell, and the stomatal pore opens (Figure 1C).

A comparative transcriptomic approach of ABA signaling in the cells of the barley stomatal complex revealed the presence of components that were well known from investigations of *Arabidopsis* GCs (Table S2). These data suggested that, in addition to the evolution of functionally linked and morphologically distinct guard and SCs, we should look for augmentation of known players in addition to novel elements to explain the rapid movements in barley stomata.

A Tandem Amino Acid Signature in Monocot SLAC1 Anion Channels Provides for Nitrate-Dependent Gating

Here, we focused on the barley SLAC1 anion channel. The regulation of this channel by ABI1 and OST1 appeared to be highly conserved between *Arabidopsis* and barley (Figures 2B and 2C [14, 15]). The most striking feature to emerge was that gating of the barley GC anion channel is controlled by ABA signaling and nitrate (Figures 2 and 3). Using a structural biology approach coupled with site-directed mutagenesis, we identified the key residues located in TMD3 that are responsible for nitrate gating (Figure 4). Interestingly, structure-function investigations with AtSLAH2 also identified serine 228 (equivalent to V273 in AtSLAC1) in TMD3 as the key residue for the strict nitrate selectivity of the root anion channel [18]. Monocot SLACs could only be converted to nitrate-independent dicot-like anion channels when TMD3 together with TMD1 and 2 were exchanged (Figures 4D–4F). This indicates that, during SLAC1 evolution in monocots, residues on TMD1 and 2 coevolved together with the IA motif in TMD3 to form the nitrate gating site (Figure 4C; Table S3). Whether and how the intrinsic nitrate sensor in monocot SLAC1 anion channels contribute to the evolutionary success of cereals remain to be shown. However, it is tempting to speculate that SLAC1 anion channels harboring an intrinsic nitrate sensor might allow the plant to integrate leaf nitrate levels and the velocity/degree of stomatal closure.

Evolution of the SLAC1 Pore Properties

We and others showed that SLAC1 channels in dicots are permeable to chloride and nitrate and do not require nitrate as gating modifier (this study and [14, 15, 17, 40]). In contrast, monocot SLAC1 channels, such as HvSLAC1, PdSLAC1, and OsSLAC1, require nitrate at the extracellular face of the anion channel pore to gate open, which is reminiscent of the nitrate-dependent gating of AtSLAH3 and PttSLAH3 anion channels [17, 31, 41, 42]. Sequence comparisons identified a VV signature in dicot and an IA signature in monocot SLACs that clearly differ between these two evolutionary distinct plant lineages (Figures S3 and S4A). Interestingly, similar to monocot SLAC1s, nitrate-activated SLAH2/3 anion channels also possess either an IA or an IS motif on TMD3 (Figure S3).

SLAC1-type anion channels are found in the most basal land plants such as green algae *Klebsormidium nitens* as well as in the liverwort *Marchantia polymorpha* [30]. With the emergence of stomata in mosses such as *Physcomitrella patens*, SLAC1 anion channels co-opted the fast ABA-signaling cascade and became OST1 sensitive [30]. Figures S3 and S4A show that the IA motif appeared in moss first and remained largely conserved until the emergence of Arecales (date palm) and Poales lineages that include important grass crops such as rice, maize, and barley. In the latter monocots, nitrate-dependent gating is fully functional (this study and [21]). This raises the question of when in evolution SLAC1-type anion channels carrying an IA motive evolved nitrate-dependent gating?

To answer this question, we analyzed the chord conductance of a set of SLAC1 anion channels derived from evolutionary distinct basal plant lineages including the moss *Physcomitrella patens*, the lycophyte *Selaginella moellendorffii*, the fern *Ceratopteris richardii*, and the seagrass *Zostera marina*. Apart from the moss PpSLAC1, all tested basal SLAC1 anion channels appeared equally nitrate insensitive as the dicot SLAC1 anion channels from *Arabidopsis*, tobacco, and tomato (Figures S4B and 2D). This may indicate that nitrate-dependent gating evolved as recently as the emergence of monocot species, although the IA motif on TMD3 is already established in a majority of SLAC-type anion channels of basal plant lineages (Figures S3 and S4A). In contrast, following the split between dicots and monocots, the SLAC1s from dicot species lost the IA signature and did not develop a nitrate-dependent gating mechanism (Figure S4A).

To further support that nitrate-dependent gating in monocot species evolved after the split between monocots and dicots, we employed a probabilistic approach [43], to infer the most probable core SLAC1 sequence (TMD1–10) of the common ancestor from which all extant dicot and monocot SLAC1s evolved (Figure S4A). This inferred core sequence was synthesized, equipped with the N- and C terminus of AtSLAC1 and named Ancestral Slow Anion Channel 1 (AncSLAC1, sequence can be found in Table S4). Interestingly, AncSLAC1 carried the IA motif on TMD3 just like monocot and basal SLAC1s. Following co-expression with CPK6 in *Xenopus leavis* oocytes, AncSLAC1 displayed typical S-type anion currents that slowly deactivated at hyperpolarized membrane potentials (Figure S4C). In line with SLAC1s from dicots but in contrast to nitrate-activated monocot SLAC1 channels, AncSLAC1 mediated macroscopic anion currents in both chloride and nitrate-based media (Figures S4B and S4C) and showed no nitrate-dependent gating behavior (Figure S4D). Thus, both the predicted common ancestor of dicot and monocot SLAC1 channels AncSLAC1 as well as SLAC1 channels from basal plant lineages were equipped with the IA motif on TMD3 but displayed a largely nitrate-independent gating behavior, suggesting that monocots have evolved the nitrate-dependent gating mechanism after the split from the dicot species. Future studies will address the question, which backbone sites had to emerge in TMD1 and/or 2 together with the IA motif to form a nitrate-sensitive SLAC1 gate in monocots?

STAR★METHODS

Detailed methods are provided in the online version of this paper and include the following:

- KEY RESOURCES TABLE
- CONTACT FOR REAGENT AND RESOURCE SHARING
- EXPERIMENTAL MODEL AND SUBJECT DETAILS
  - Plant material and growth conditions
  - *Xenopus* oocyte preparation
- METHODS DETAILS
  - RNA sequencing
  - RNA-seq data analysis
  - Functional annotation of barley
  - Gas exchange experiments
  - qPCR
  - Energy dispersive X-ray analysis
  - Cloning and cRNA synthesis
  - Protein-protein interaction studies
  - Oocyte recordings
  - Evolutionary coupling analysis
  - Frequency logos of TMD1 to 3
  - Alignment, phylogenetic analysis and inference of ancestral SLAC1
- QUANTIFICATION AND STATISTICAL ANALYSES
- DATA AND SOFTWARE AVAILABILITY
  - Accession numbers

SUPPLEMENTAL INFORMATION

Supplemental Information includes four figures and five tables and can be found with this article online at https://doi.org/10.1016/j.cub.2018.03.027.

ACKNOWLEDGMENTS

This work was funded by Bavarian State Ministry of the Environment and Consumer Protection. R.H. and D.G. were supported by the German Research Foundation (DFG) within the CRC/TR166 ''ReceptorLight'' project B8 and by the King Saud University, Saudi Arabia. M.E.J. is supported by a grant from the Danish Council for Independent Research: DFF–6108-00122. We thank Andreas Ruth for *Zostera marina* plant material and Ingo Dreyer for initial analysis of signatures in SLAC1 isoforms. A.M.H. acknowledges support from the BBSRC.

AUTHOR CONTRIBUTIONS

P.A., M.F., J.H., M.E.J., C.L., S.L., T.M., K.v.M., and N.S. performed the research and analyzed the data. T.M., M.E.J., P.A., D.G., A.M.H., and R.H. designed the study. T.M., M.E.J., P.A., J.F., D.G., A.M.H., and R.H. wrote the manuscript.

DECLARATION OF INTERESTS

The authors declare no competing interests.

Received: October 30, 2017
Revised: February 5, 2018
Accepted: March 14, 2018
Published: April 26, 2018

REFERENCES

1. Hedrich, R. (2012). Ion channels in plants. Physiol. Rev. *92*, 1777–1811.
2. Hedrich, R., and Geiger, D. (2017). Biology of SLAC1-type anion channels—From nutrient uptake to stomatal closure. New Phytol. *216*, 46–61.
3. Munemasa, S., Hauser, F., Park, J., Waadt, R., Brandt, B., and Schroeder, J.I. (2015). Mechanisms of abscisic acid-mediated control of stomatal aperture. Curr. Opin. Plant Biol. *28*, 154–162.
4. Chen, Z.H., Chen, G., Dai, F., Wang, Y., Hills, A., Ruan, Y.L., Zhang, G., Franks, P.J., Nevo, E., and Blatt, M.R. (2017). Molecular evolution of grass stomata. Trends Plant Sci. *22*, 124–139.
5. Shen, L., Sun, P., Bonnell, V.C., Edwards, K.J., Hetherington, A.M., McAinsh, M.R., and Roberts, M.R. (2015). Measuring stress signaling responses of stomata in isolated epidermis of graminaceous species. Front. Plant Sci. *6*, 533.
6. Raissig, M.T., Matos, J.L., Anleu Gil, M.X., Kornfeld, A., Bettadapur, A., Abrash, E., Allison, H.R., Badgley, G., Vogel, J.P., Berry, J.A., and Bergmann, D.C. (2017). Mobile MUTE specifies subsidiary cells to build physiologically improved grass stomata. Science *355*, 1215–1218.
7. Kusumi, K., Hashimura, A., Yamamoto, Y., Negi, J., and Iba, K. (2017). Contribution of the S-type anion channel SLAC1 to stomatal control and its dependence on developmental stage in rice. Plant Cell Physiol. *58*, 2085–2094.
8. Sun, S.J., Qi, G.N., Gao, Q.F., Wang, H.Q., Yao, F.Y., Hussain, J., and Wang, Y.F. (2016). Protein kinase OsSAPK8 functions as an essential activator of S-type anion channel OsSLAC1, which is nitrate-selective in rice. Planta *243*, 489–500.
9. Raschke, K., and Fellows, M.P. (1971). Stomatal movement in Zea mays: Shuttle of potassium and chloride between guard cells and subsidiary cells. Planta *101*, 296–316.
10. Ma, Y., Szostkiewicz, I., Korte, A., Moes, D., Yang, Y., Christmann, A., and Grill, E. (2009). Regulators of PP2C phosphatase activity function as abscisic acid sensors. Science *324*, 1064–1068.
11. Park, S.Y., Fung, P., Nishimura, N., Jensen, D.R., Fujii, H., Zhao, Y., Lumba, S., Santiago, J., Rodrigues, A., Chow, T.F., et al. (2009). Abscisic acid inhibits type 2C protein phosphatases via the PYR/PYL family of START proteins. Science *324*, 1068–1071.
12. Soon, F.F., Ng, L.M., Zhou, X.E., West, G.M., Kovach, A., Tan, M.H., Suino-Powell, K.M., He, Y., Xu, Y., Chalmers, M.J., et al. (2012). Molecular mimicry regulates ABA signaling by SnRK2 kinases and PP2C phosphatases. Science *335*, 85–88.
13. Fujii, H., Chinnusamy, V., Rodrigues, A., Rubio, S., Antoni, R., Park, S.Y., Cutler, S.R., Sheen, J., Rodriguez, P.L., and Zhu, J.K. (2009). In vitro reconstitution of an abscisic acid signalling pathway. Nature *462*, 660–664.
14. Geiger, D., Scherzer, S., Mumm, P., Stange, A., Marten, I., Bauer, H., Ache, P., Matschi, S., Liese, A., Al-Rasheid, K.A., et al. (2009). Activity of guard cell anion channel SLAC1 is controlled by drought-stress signaling kinase-phosphatase pair. Proc. Natl. Acad. Sci. USA *106*, 21425–21430.
15. Lee, S.C., Lan, W., Buchanan, B.B., and Luan, S. (2009). A protein kinase-phosphatase pair interacts with an ion channel to regulate ABA signaling in plant guard cells. Proc. Natl. Acad. Sci. USA *106*, 21419–21424.
16. Ache, P., Becker, D., Ivashikina, N., Dietrich, P., Roelfsema, M.R., and Hedrich, R. (2000). GORK, a delayed outward rectifier expressed in guard cells of Arabidopsis thaliana, is a K(+)-selective, K(+)-sensing ion channel. FEBS Lett. *486*, 93–98.
17. Geiger, D., Maierhofer, T., Al-Rasheid, K.A., Scherzer, S., Mumm, P., Liese, A., Ache, P., Wellmann, C., Marten, I., Grill, E., et al. (2011). Stomatal closure by fast abscisic acid signaling is mediated by the guard cell anion channel SLAH3 and the receptor RCAR1. Sci. Signal. *4*, ra32.
18. Maierhofer, T., Lind, C., Hüttl, S., Scherzer, S., Papenfuß, M., Simon, J., Al-Rasheid, K.A., Ache, P., Rennenberg, H., Hedrich, R., et al. (2014). A Single-Pore Residue Renders the Arabidopsis Root Anion Channel SLAH2 Highly Nitrate Selective. Plant Cell *26*, 2554–2567.
19. Brandt, B., Brodsky, D.E., Xue, S., Negi, J., Iba, K., Kangasjärvi, J., Ghassemian, M., Stephan, A.B., Hu, H., and Schroeder, J.I. (2012). Reconstitution of abscisic acid activation of SLAC1 anion channel by CPK6 and OST1 kinases and branched ABI1 PP2C phosphatase action. Proc. Natl. Acad. Sci. USA *109*, 10593–10598.
20. Amien, S., Kliwer, I., Márton, M.L., Debener, T., Geiger, D., Becker, D., and Dresselhaus, T. (2010). Defensin-like ZmES4 mediates pollen tube burst in maize via opening of the potassium channel KZM1. PLoS Biol. *8*, e1000388.
21. Müller, H.M., Schäfer, N., Bauer, H., Geiger, D., Lautner, S., Fromm, J., Riederer, M., Bueno, A., Nussbaumer, T., Mayer, K., et al. (2017). The desert plant Phoenix dactylifera closes stomata via nitrate-regulated SLAC1 anion channel. New Phytol. *216*, 150–162.
22. Büchsenschütz, K., Marten, I., Becker, D., Philippar, K., Ache, P., and Hedrich, R. (2005). Differential expression of K+ channels between guard cells and subsidiary cells within the maize stomatal complex. Planta *222*, 968–976.
23. Fricke, W., Pritchard, J., Leigh, R.A., and Tomos, A.D. (1994). Cells of the upper and lower epidermis of barley (Hordeum vulgare L.) leaves exhibit distinct patterns of vacuolar solutes. Plant Physiol. *104*, 1201–1208.
24. Yamauchi, S., Takemiya, A., Sakamoto, T., Kurata, T., Tsutsumi, T., Kinoshita, T., and Shimazaki, K. (2016). The plasma membrane H+-ATPase AHA1 plays a major role in stomatal opening in response to blue light. Plant Physiol. *171*, 2731–2743.
25. Bauer, H., Ache, P., Lautner, S., Fromm, J., Hartung, W., Al-Rasheid, K.A., Sonnewald, S., Sonnewald, U., Kneitz, S., Lachmann, N., et al. (2013). The stomatal response to reduced relative humidity requires guard cell-autonomous ABA synthesis. Curr. Biol. *23*, 53–57.
26. Belin, C., de Franco, P.O., Bourbousse, C., Chaignepain, S., Schmitter, J.M., Vavasseur, A., Giraudat, J., Barbier-Brygoo, H., and Thomine, S. (2006). Identification of features regulating OST1 kinase activity and OST1 function in guard cells. Plant Physiol. *141*, 1316–1327.
27. Boudsocq, M., Droillard, M.J., Barbier-Brygoo, H., and Laurière, C. (2007). Different phosphorylation mechanisms are involved in the activation of -sucrose non-fermenting 1 related protein kinases 2 by osmotic stresses and abscisic acid. Plant Mol. Biol. *63*, 491–503.
28. Yoshida, R., Umezawa, T., Mizoguchi, T., Takahashi, S., Takahashi, F., and Shinozaki, K. (2006). The regulatory domain of SRK2E/OST1/SnRK2.6 interacts with ABI1 and integrates abscisic acid (ABA) and osmotic stress signals controlling stomatal closure in Arabidopsis. J. Biol. Chem. *281*, 5310–5318.
29. McAdam, S.A., Brodribb, T.J., Banks, J.A., Hedrich, R., Atallah, N.M., Cai, C., Geringer, M.A., Lind, C., Nichols, D.S., Stachowski, K., et al. (2016). Abscisic acid controlled sex before transpiration in vascular plants. Proc. Natl. Acad. Sci. USA *113*, 12862–12867.
30. Lind, C., Dreyer, I., López-Sanjurjo, E.J., von Meyer, K., Ishizaki, K., Kohchi, T., Lang, D., Zhao, Y., Kreuzer, I., Al-Rasheid, K.A., et al. (2015). Stomatal guard cells co-opted an ancient ABA-dependent desiccation survival system to regulate stomatal closure. Curr. Biol. *25*, 928–935.
31. Maierhofer, T., Diekmann, M., Offenborn, J.N., Lind, C., Bauer, H., Hashimoto, K., S Al-Rasheid, K.A., Luan, S., Kudla, J., Geiger, D., and Hedrich, R. (2014). Site- and kinase-specific phosphorylation-mediated activation of SLAC1, a guard cell anion channel stimulated by abscisic acid. Sci. Signal. *7*, ra86.
32. Scherzer, S., Maierhofer, T., Al-Rasheid, K.A., Geiger, D., and Hedrich, R. (2012). Multiple calcium-dependent kinases modulate ABA-activated guard cell anion channels. Mol. Plant *5*, 1409–1412.

33. Desikan, R., Griffiths, R., Hancock, J., and Neill, S. (2002). A new role for an old enzyme: Nitrate reductase-mediated nitric oxide generation is required for abscisic acid-induced stomatal closure in Arabidopsis thaliana. Proc. Natl. Acad. Sci. USA *99*, 16314–16318.

34. Kawachi, T., Shoji, Y., Sugimoto, T., Oji, Y.L., Kleinhofs, A., Warner, R.L., Ohtake, N., Ohyama, T., and Sueyoshi, K. (2002). Role of xylem sap nitrate in the regulation of nitrate reductase gene expression in leaves of barley (Hordeum vulgare L.) seedlings. Soil Sci. Plant Nutr. *48*, 79–85.

35. Sueyoshi, K., Kleinhofs, A., and Warner, R.L. (1995). Expression of NADH-specific and NAD(P)H-bispecific nitrate reductase genes in response to nitrate in barley. Plant Physiol. *107*, 1303–1311.

36. Chen, Y.H., Hu, L., Punta, M., Bruni, R., Hillerich, B., Kloss, B., Rost, B., Love, J., Siegelbaum, S.A., and Hendrickson, W.A. (2010). Homologue structure of the SLAC1 anion channel for closing stomata in leaves. Nature *467*, 1074–1080.

37. Humphrey, W., Dalke, A., and Schulten, K. (1996). VMD: Visual molecular dynamics. J. Mol. Graph *14*, 33–38.

38. Franks, P.J., and Farquhar, G.D. (2007). The mechanical diversity of stomata and its significance in gas-exchange control. Plant Physiol. *143*, 78–87.

39. Hetherington, A.M., and Woodward, F.I. (2003). The role of stomata in sensing and driving environmental change. Nature *424*, 901–908.

40. Geiger, D., Scherzer, S., Mumm, P., Marten, I., Ache, P., Matschi, S., Liese, A., Wellmann, C., Al-Rasheid, K.A., Grill, E., et al. (2010). Guard cell anion channel SLAC1 is regulated by CDPK protein kinases with distinct Ca2+ affinities. Proc. Natl. Acad. Sci. USA *107*, 8023–8028.

41. Jaborsky, M., Maierhofer, T., Olbrich, A., Escalante-Pérez, M., Müller, H.M., Simon, J., Krol, E., Cuin, T.A., Fromm, J., Ache, P., et al. (2016). SLAH3-type anion channel expressed in poplar secretory epithelia operates in calcium kinase CPK-autonomous manner. New Phytol. *210*, 922–933.

42. Demir, F., Horntrich, C., Blachutzik, J.O., Scherzer, S., Reinders, Y., Kierszniowska, S., Schulze, W.X., Harms, G.S., Hedrich, R., Geiger, D., and Kreuzer, I. (2013). Arabidopsis nanodomain-delimited ABA signaling pathway regulates the anion channel SLAH3. Proc. Natl. Acad. Sci. USA *110*, 8296–8301.

43. Ashkenazy, H., Penn, O., Doron-Faigenboim, A., Cohen, O., Cannarozzi, G., Zomer, O., and Pupko, T. (2012). FastML: A web server for probabilistic reconstruction of ancestral sequences. Nucleic Acids Res. *40*, W580–W584.

44. Usadel, B., Poree, F., Nagel, A., Lohse, M., Czedik-Eysenberg, A., and Stitt, M. (2009). A guide to using MapMan to visualize and compare Omics data in plants: A case study in the crop species, Maize. Plant Cell Environ. *32*, 1211–1229.

45. An, Y.Q., McDowell, J.M., Huang, S., McKinney, E.C., Chambliss, S., and Meagher, R.B. (1996). Strong, constitutive expression of the Arabidopsis ACT2/ACT8 actin subclass in vegetative tissues. Plant J. *10*, 107–121.

46. Nour-Eldin, H.H., Hansen, B.G., Nørholm, M.H., Jensen, J.K., and Halkier, B.A. (2006). Advancing uracil-excision based cloning towards an ideal technique for cloning PCR fragments. Nucleic Acids Res. *34*, e122.

47. Kim, D., Langmead, B., and Salzberg, S.L. (2015). HISAT: A fast spliced aligner with low memory requirements. Nat. Methods *12*, 357–360.

48. Liao, Y., Smyth, G.K., and Shi, W. (2014). featureCounts: An efficient general purpose program for assigning sequence reads to genomic features. Bioinformatics *30*, 923–930.

49. Hopf, T.A., Colwell, L.J., Sheridan, R., Rost, B., Sander, C., and Marks, D.S. (2012). Three-dimensional structures of membrane proteins from genomic sequencing. Cell *149*, 1607–1621.

50. Marks, D.S., Colwell, L.J., Sheridan, R., Hopf, T.A., Pagnani, A., Zecchina, R., and Sander, C. (2011). Protein 3D structure computed from evolutionary sequence variation. PLoS ONE *6*, e28766.

51. Altschul, S.F., Gish, W., Miller, W., Myers, E.W., and Lipman, D.J. (1990). Basic local alignment search tool. J. Mol. Biol. *215*, 403–410.

52. Edgar, R.C. (2004). MUSCLE: Multiple sequence alignment with high accuracy and high throughput. Nucleic Acids Res. *32*, 1792–1797.

53. Crooks, G.E., Hon, G., Chandonia, J.M., and Brenner, S.E. (2004). WebLogo: A sequence logo generator. Genome Res. *14*, 1188–1190.

54. Pettersen, E.F., Goddard, T.D., Huang, C.C., Couch, G.S., Greenblatt, D.M., Meng, E.C., and Ferrin, T.E. (2004). UCSF Chimera–a visualization system for exploratory research and analysis. J. Comput. Chem. *25*, 1605–1612.

55. Clamp, M., Cuff, J., Searle, S.M., and Barton, G.J. (2004). The Jalview Java alignment. Bioinformatics *20*, 426–427.

56. Huelsenbeck, J.P., and Ronquist, F. (2001). MRBAYES: Bayesian inference of phylogenetic trees. Bioinformatics *17*, 754–755.

57. Darriba, D., Taboada, G.L., Doallo, R., and Posada, D. (2011). ProtTest 3: Fast selection of best-fit models of protein evolution. Bioinformatics *27*, 1164–1165.

58. Stamatakis, A. (2014). RAxML version 8: a tool for phylogenetic analysis and post-analysis of large phylogenics. Bioinformatics *30*, 1312–1313.

59. Mascher, M., Gundlach, H., Himmelbach, A., Beier, S., Twardziok, S.O., Wicker, T., Radchuk, V., Dockter, C., Hedley, P.E., Russell, J., et al. (2017). A chromosome conformation capture ordered sequence of the barley genome. Nature *544*, 427–433.

60. Wagner, G.P., Kin, K., and Lynch, V.J. (2012). Measurement of mRNA abundance using RNA-seq data: RPKM measure is inconsistent among samples. Theory Biosci. *131*, 281–285.

61. Arabidopsis Genome, I.; Arabidopsis Genome Initiative (2000). Analysis of the genome sequence of the flowering plant Arabidopsis thaliana. Nature *408*, 796–815.

62. Szyroki, A., Ivashikina, N., Dietrich, P., Roelfsema, M.R., Ache, P., Reintanz, B., Deeken, R., Godde, M., Felle, H., Steinmeyer, R., et al. (2001). KAT1 is not essential for stomatal opening. Proc. Natl. Acad. Sci. USA *98*, 2917–2921.

63. Dadacz-Narloch, B., Beyhl, D., Larisch, C., López-Sanjurjo, E.J., Reski, R., Kuchitsu, K., Müller, T.D., Becker, D., Schönknecht, G., and Hedrich, R. (2011). A novel calcium binding site in the slow vacuolar cation channel TPC1 senses luminal calcium levels. Plant Cell *23*, 2696–2707.

64. Nørholm, M.H. (2010). A mutant Pfu DNA polymerase designed for advanced uracil-excision DNA engineering. BMC Biotechnol. *10*, 21.

65. Geu-Flores, F., Nour-Eldin, H.H., Nielsen, M.T., and Halkier, B.A. (2007). USER fusion: A rapid and efficient method for simultaneous fusion and cloning of multiple PCR products. Nucleic Acids Res. *35*, e55.

66. Jørgensen, M.E., Xu, D., Crocoll, C., Ramírez, D., Motawia, M.S., Olsen, C.E., Nour-Eldin, H.H., and Halkier, B.A. (2017). Origin and evolution of transporter substrate specificity within the NPF family. eLife *6*, e19466.

67. Le, S.Q., and Gascuel, O. (2008). An improved general amino acid replacement matrix. Mol. Biol. Evol. *25*, 1307–1320.

68. Reeves, J.H. (1992). Heterogeneity in the substitution process of amino acid sites of proteins coded for by mitochondrial DNA. J. Mol. Evol. *35*, 17–31.

69. Yang, Z. (1993). Maximum-likelihood estimation of phylogeny from DNA sequences when substitution rates differ over sites. Mol. Biol. Evol. *10*, 1396–1401.

70. Miller, M.A., Pfeiffer, W., and Schwartz, T. (2011). The CIPRES science gateway: A community resource for phylogenetic analyses. In Proceedings of the 2011 TeraGrid Conference: Extreme Digital Discovery (ACM), pp. 1–8.

STAR★METHODS

KEY RESOURCES TABLE

REAGENT or RESOURCE	SOURCE	IDENTIFIER
Bacterial and Virus Strains		
XL1-Blue MRF' *E. coli* Strain used for cloning	Widely distributed	N/A
Biological Samples		
Hordeum vulgare cultivar Barke	Saatzucht J. Breun GmbH & Co. KG, Herzogenaurach, Germany	N/A
Chemicals, Peptides, and Recombinant Proteins		
(±)-Abscisic acid (ABA)	Sigma-Aldrich, Merck	Catalog #A1049
Gentamicin sulfate salt	Sigma-Aldrich, Merck	Catalog #G1264
Standard chemicals such as salts and buffers for oocyte recordings or for molecular biology	Sigma-Aldrich, Merck	N/A
USER-Enzyme for advanced uracil-excision-based cloning and USER fusion technique [44, 45],	New England Biolabs	Catalog #M5505
Critical Commercial Assays		
NucleoSpin® RNA Plant Kit	Macherey-Nagel, Germany	Catalog #740949.250
TruSeq RNA Library Prep Kit v2	Illumina, San Diego, CA, USA	Catalog #RS-122-2001
AmpliCap-Max T7 High Yield Message Maker Kit	Cellscript, Madison, WI, USA	Catalog #C-MSC100625
Deposited Data		
Raw RNA-seq sequence reads	This paper, *Hordeum vulgare* cultivar Barke	European Nucleotide Archive with accession number ArrayExpress accession E-MTAB-5877
HvSLAC1 sequence	Hordeum vulgare cultivar Barke; this paper	Accession#: MF197384
Crystal Structure of Plant SLAC1 homolog TehA	[36]	PDP: 3M71
Experimental Models: Organisms/Strains		
Hordeum vulgare cultivar Barke	Saatzucht J. Breun GmbH & Co. KG, Herzogenaurach, Germany	N/A
Oligonucleotides		
For qPCR primers see Table S5	synthesized by TIB Molbiol Berlin, Germany	This paper
Recombinant DNA		
Oocyte expression vector	[46]	pNB1u
Oocyte expression vector for C-terminal fusions to the C-terminal part of YFP for use in BiFC	[46]	pNB1uYC
Oocyte expression vector for C-terminal fusions to the N-terminal part of YFP for use in BiFC	[46]	pNB1uYN
Coding sequences of XySLAC/SLAH anion channels and mutants/chimera thereof were cloned into pNB1u or pNB1uYC for electrophysiological analysis or BiFC-based interaction studies in *X. leavis* oocytes. Xy represent the identifiers of the respective species where the SLAC1 anion channel originates from.	This study [14, 40]	N/A
Coding sequences of AtCPK6, AtOST1, AtABI1 and mutants thereof were cloned into pNB1u or pNB1uYN for electrophysiological analysis or BiFC-based interaction studies in *X. leavis* oocytes.	This study [14, 40]	N/A
Software and Algorithms		
FASTQC v0.10.1	Babraham Bioinformatics, Simon Andrews	http://www.bioinformatics.babraham.ac.uk/projects/fastqc/
Hisat2 (hisat2-2.0.3-beta)	https://ccb.jhu.edu/software/hisat2/index.shtml	[47]

(*Continued on next page*)

Continued

REAGENT or RESOURCE	SOURCE	IDENTIFIER
Subread software package (Subread-1.4.6)	https://sourceforge.net/projects/subread/?source=navbar	[48]
EVfold/EVcouplings	http://evfold.org/evfold-web/evfold.do	[49, 50]
VMD	http://www.ks.uiuc.edu/Research/vmd/	[37]
BLASTP	https://blast.ncbi.nlm.nih.gov/Blast.cgi?PAGE=Proteins	[51]
MUSCLE	http://www.drive5.com/muscle/	[52]
Weblogo	http://weblogo.berkeley.edu/logo.cgi	[53]
Chimera	http://www.cgl.ucsf.edu/chimera/index.html	[54]
Jalview	http://www.jalview.org/	[55]
MrBayes 3.2.6	http://mrbayes.sourceforge.net/download.php	[56]
Prottest v3.4.2	https://github.com/ddarriba/prottest3	[57]
RAxML 8.2.9	https://github.com/stamatak/standard-RAxML	[58]
figtree	http://tree.bio.ed.ac.uk/software/figtree/	N/A
FastML	http://fastml.tau.ac.il/source.html	[43]

CONTACT FOR REAGENT AND RESOURCE SHARING

Further information and requests for resources and reagents should be directed to and will be fulfilled by the Lead Contact, Dietmar Geiger (geiger@botanik.uni-wuerzburg.de).

EXPERIMENTAL MODEL AND SUBJECT DETAILS

Plant material and growth conditions

Barley (*Hordeum vulgare* cv. Barke) seeds were provided by a commercial supplier (Saatzucht J. Breun GmbH & Co. KG) and cultivated at 22/16°C and 50 ± 5% RH at a 12/12h day/night cycle and a photon flux density of 500 μmol m-2 s-1 white light (Philips Master T Green Powers, 400 W).

Xenopus oocyte preparation

Investigations on SLAC1 anion channels were performed in oocytes of the African clawfrog *Xenopus laevis*. Permission for keeping *Xenopus* exists at the Julius-von-Sachs Institute and is registered at the government of Lower Franconia (reference number 70/14). Mature female *Xenopus laevis* frogs (healthy, non-immunized and not involved in any previous procedures) were kept at 20°C at a 12/12h day/night cycle in dark gray 96 l tanks (5 frogs/tank). Frogs were fed twice a week with floating trout food (Fisch-Fit Mast 45/7 2mm, Interquell GmbH, Wehringen, Germany). Tanks are equipped with 30 cm long PVC pipes with a diameter of around 10 cm. These pipes are used as hiding places for the frogs. The water is continuously circulated and filtered by a small aquarium pump. For oocyte isolation, mature female *X. laevis* frogs were anesthetized by immersion in water containing 0.1% 3-aminobenzoic acid ethyl ester. Following partial ovariectomy, stage V or VI oocytes were treated with 0.14 mg/ml collagenase I in Ca^{2+}-free ND96 buffer (10 mM HEPES pH 7.4, 96 mM NaCl, 2 mM KCl, 1 mM $MgCl_2$,) for 1.5 h. Subsequently, oocytes were washed with Ca^{2+}-free ND96 buffer and kept at 16°C in ND96 solution (10 mM HEPES pH 7.4, 96 mM NaCl, 2 mM KCl, 1 mM $MgCl_2$, 1mM $CaCl_2$) containing 50mg/l gentamycin. For oocyte BiFC and electrophysiological experiments 10 ng of each cRNA was injected into selected oocytes. Oocytes were incubated for 2 days at 16°C in ND96 solution containing gentamycin.

METHODS DETAILS

RNA sequencing

Epidermal peels were collected from the abaxial side of 8 to 10-day-old leaves. To prepare isolated epidermal peels [5], leaves were cut from the plant and bent over the forefinger with the adaxial surface facing upward. A shallow cut was made with a sharp razor blade horizontally across the leaf and a flap of leaf tissue lifted with a razor, leaving the lower epidermis intact. The leaf tissue was removed from the epidermis with forceps. RNA was extracted from a total of 20 epidermal peels per sample using the NucleoSpin® RNA Plant Kit (Macherey-Nagel,Drueren, Germany). RNA isolation from whole leaves was performed similarly.

The extracted RNA was treated with RNase-free DNase (New England Biolabs, Ipswich, MA, USA). Quality control measurements were performed on a 2100 Bioanalyzer (Agilent, Santa Clara, CA, USA) and the concentration was determined using a Nanodrop ND-1000 spectrophotometer (Thermo Fisher Scientific, Wilmington, DE, USA). Following RNA isolation, we sequenced RNA of one sample, each to get a first overview of genes in barley GC complexes that are known to be involved in stomatal movements.

In addition, we were thus able to obtain the sequence information for cloning selected transporters and channels. Libraries were prepared with the TruSeq RNA Sample Prep Kit v2 (Illumina, San Diego, CA, USA) using 1 μg of RNA and sequenced on a HiSeq 3000 (Illumina) resulting in a sequence depth of 35 million paired-end reads (2x 150bp).

RNA-seq data analysis

Sequencing adaptors were initially removed, and the overall high quality of the remaining reads was confirmed using FastQC (FASTQC v0.10.1, Andrews: http://www.bioinformatics.babraham.ac.uk/projects/fastqc/) (average Phred quality score of > 30 across all bases at each position in the FastQ files). Subsequently, reads were aligned to the barley reference assembly [59] using Hisat2 (hisat2-2.0.3-beta) [47] by applying default settings for paired-end data. The featureCounts function of the subread-1.4.6 package [48] was used to generate counts for high-confidence genes of barley [59]. Only uniquely mapped read pairs were counted. Data normalization was performed by calculating TPM (Transcripts Per Kilobase Million) [60] values.

Functional annotation of barley

The functional annotation of the barley genes was provided by Mascher et al. (2017 [59]). Best hits of a BLASTP [51] alignment of barley high-confidence protein sequences against the *A. thaliana* protein sequences (TAIR10 [61],) were used to assign *A. thaliana* genes and the corresponding MapMan categories [44] to barley genes.

Gas exchange experiments

For gas exchange measurements [21], we used detached leaves of 8 to 10-day-old *Hordeum vulgare* cv. Barke. The leaves were cut under water to avoid xylem embolism and immediately placed in deionized water or 5 mM KNO_3 and kept there for the whole measurement period. The effect of ABA application with or without KNO_3 on the transpirational water loss was measured at a photon flux density of 500 μmol $m^{-2}s^{-1}$. After stabilization of the transpiration ABA with a final concentration of 25 μM was fed into the water reservoir containing either deionized water or 5 mM KNO_3. Transpirational water loss was measured under constant conditions: air humidity of 52.5%, temperature of 20°C, and a photon flux density of 500 μmol m^{-2} s^{-1}.

qPCR

Quantitative PCR (qPCR) experiments were performed with samples taken from whole leaves epidermal peels and highly GC enriched tissue. Epidermal peels from 12-day-old Barley (cv. Barke) leaves were isolated according to [5]. Thereby only the GC SC complex survives. For GC samples we used the "blender method" on epidermal peels with mature, intact GCs to mechanically and selectively destroy the SCs while keeping GCs alive. GC were enriched within 8 minutes by successive blender cycles (45 s each) in ice-cold deionized water with additional crushed ice and filtered through a 210-μm nylon mash. After two rounds of blending, the remaining light green epidermal fraction was further processed. Neutral red staining indicated that at least 90% of the viable cells in the preparations were GCs. Total RNA from at least three individual biological replicates was prepared using the NucleoSpin® RNA Plant Kit (Macherey Nagel, Drueren, Germany) and stored for subsequent microarray hybridizations or qPCR.

For qPCR potential DNA contamination was removed from total RNA by treatment with RNase-Free DNase I (Thermo Scientific, Waltham MA) according to the manufacturer's protocol. First-strand cDNA was prepared using 2.5 μg RNA with the M-MLV-RT kit (Promega, Mannheim, Germany). First-strand cDNA samples were 20-fold diluted in water and subjected to qPCR using a Mastercycler® ep Realplex2S (Eppendorf) with the ABsolute SYBR Capillary Mix (Thermo Scientific, Waltham MA) in 20 μl reaction volumes. Primers used (TIB MOLBIOL, Germany) have been designed according to the sequences from the RNA-seq analyses and validated prior to qPCR. All primers were chosen to amplify fragments not exceeding 500 base pairs. Each transcript was quantified using individual standards. To enable detection of contaminating genomic DNA, PCR was performed with the same RNA as template that was used for cDNA synthesis. Transcripts were each normalized to 10.000 molecules of barley actin4/1. These barley actin fragments, used as house-keeping genes, were homologous to actins 2 and 8 constitutively expressed in most *Arabidopsis* tissues (for details see [45, 62]. All kits were used according to the manufacturer's protocols. The primers are listed in the Key Resources Table.

Energy dispersive X-ray analysis

Leaf samples with open and closed stomata were prepared using the gas exchange setup. Cut leaves were either treated with opening conditions (500 μmol m^{-2} s^{-1} light, 0 ppm CO_2) or closing conditions (darkness, 1000 ppm CO_2) until the transpirational water loss stabilized. The samples were then immediately frozen in liquid nitrogen and lyophilized over a period of 3 days in an ice condenser (Alpha 1-2, Christ GmbH, Germany) under vacuum (R25, Vacuubrand GmbH & CO. KG, Germany) at −55°C. After the following freeze-drying process leaves were coated with carbon before being examined by a scanning electron microscope (SEM, S-520 Hitachi, Tokyo, Japan) equipped with an energy dispersive X-ray device (EDX eumex Si(Li)-detector, EUMEX GV, Mainz, Germany). Single-point measurements on GCs as well as on SCs were performed at 10 keV excitation energy, which excites a measurement area of < 2 μm in diameter. Element concentration provided by the analysis data represents the atomic ratio of the analyzed ions in percent.

Cloning and cRNA synthesis

The complementary DNAs (cDNAs) of various SLAC1 anion channels, AtSLAH2, AtCPK6, AtABI1 and AtOST1 were cloned into oocyte expression vectors or BiFC expression vectors (both are based on pGEM vectors), by an advanced uracil-excision-based cloning technique as described by [46]. Site-directed mutations were introduced by means of a modified USER fusion method as described by [63, 64]. In brief, the coding sequence of the respective anion channel or kinase within an oocyte expression vector (based on pNBIu vectors, see Key Resources Table) was used as a template for USER mutagenesis. Overlapping primer pairs (overlap covering 8 to 14 bp including the mutagenesis site, see Table S5) were designed [46]. PCR conditions were essentially as described by Nørholm (2010 [64]) using PfuX7 polymerase. PCR products were treated with the USER enzyme (New England Biolabs, Ipswich, MA, USA) to remove the uracil residues, generating single-stranded overlapping ends. Following uracil excision, recirculation of the plasmid was performed at 37°C for 30 minutes followed by 30 minutes at room temperature, and then constructs were immediately transformed into chemical competent *Escherichia coli* cells (XL1-Blue MRF'). All mutants were verified by sequencing [63]. The cDNA of *Arabidopsis*/barley chimeras was also cloned into oocyte expression vectors using a combination of the advanced uracil-excision-based cloning technique and the USER fusion technique [46, 65]. Primers are listed in Table S5. For functional analysis, complementary RNA (cRNA) was prepared with the AmpliCap-Max T7 High Yield Message Maker Kit (Cellscript, Madison, WI, USA). Oocyte preparation and cRNA injection is described in Experimental Model and Subject Details.

Protein-protein interaction studies

For documentation of the oocyte protein-protein interaction study (BiFC) results, pictures were taken with a Leica SP5 confocal laser scanning microscope (Leica Microsystems CMS GmbH, Mannheim, Germany) equipped with multiphoton laser of the Mai Tai-Series (Spectra Physics, Santa Clara, USA) and a Leica HCX IRAPO L25 × /0.95W objective.

Oocyte recordings

In double-electrode voltage-clamp studies, oocytes were perfused with Tris/Mes-based buffers. The standard solution contained 10 mM Tris/Mes (pH 5.6), 1 mM $Ca(gluconate)_2$, 1 mM $Mg(gluconate)_2$, 1 mM $LaCl_3$ and 100 mM NaCl, $NaNO_3$ or Na(gluconate). To balance the ionic strength, we compensated for changes in the nitrate or chloride concentration with Na(gluconate). Solutions for anion selectivity measurements were composed of 50 mM $malate^-$, $sulfate^{2-}$, Cl^-, NO_3^- or $gluconate^-$, 1 mM $Ca(gluconate)_2$; 1 mM $Mg(gluconate)_2$; and 10 mM Tris/Mes (pH 7.5). Osmolality was adjusted to 220 mosmol/kg with D-sorbitol. For recording representative current traces, steady-state currents (I_{SS}) and for calculating the voltage dependent relative open probability (rel. P_O) standard voltage protocol was as follows: Starting from a holding potential (V_H) of 0 mV, single-voltage pulses were applied in 20 mV decrements from +40 to −200 mV. Rel. P_O was calculated from a −120 mV voltage pulse following the test pulses of the standard voltage protocol by fitting the experimental data points with a Boltzmann Equation [31] of the form: rel. P_O = offset + 1 / (1 + exp ($V_{1/2}$ – V_m) / z), where $V_{1/2}$ is the half maximal activation voltage, V_m is the membrane potential and z is the slope of the Boltzmann function. The currents were normalized to the saturation value of the calculated Boltzmann distribution. Instantaneous currents (I_{inst}) were extracted immediately after the voltage jump from the holding potential of 0 mV to 50 ms test pulses ranging from +70 to −150 mV. The reversal potentials (V_{rev}) used for the calculation of the rel. permeability were recorded in the current-clamp mode [18]. For determination of V_{rev} for the respective anion, oocytes were preincubated in 50 mM NO_3^- to gain full activity of the channel. The relative permeability was calculated as described in [36] using the following equation:

$(P_X/P_{NO3}) = ([NO_3^-]_o/[X^-]_o)e^{(E_X-E_{NO3})F/RT}$ for monovalent anions and $(P_X/P_{NO3}) = ([NO_3^-]_o/4[X^{2-}]_o)e^{(E_X-E_{NO3})F/RT}(e^{-E_XF/RT}+1)$ for anions differing in valence (divalent and monovalent). $[NO_3^-]_o$ is the external concentration of the control (nitrate-based) solution and $[X^-]_o$ is the external concentration of the test anion. E_{NO3} is the reversal potential with nitrate and E_X is the reversal potential for the external test anion. F and R are the Faraday and gas constants, respectively, and T is the absolute temperature.

To calculate the chord conductance, the reversal potential (V_{rev}) was determined by fitting the instantaneous currents in chloride- and nitrate-containing standard buffers with a linear function. Using the instantaneous currents at –120 mV, the chord conductance could be calculated with the equation $g_{anion} = I_{anion} / (V - V_{rev})$ [31].

Evolutionary coupling analysis

EVfold/EVcouplings (http://evfold.org/evfold-web/evfold.do) [49, 50], a publicly available bioinformatics server, was used to predict evolutionary couplings of the amino acid residues V272 an V273 in AtSLAC1. We used the default transmembrane protein settings and the DI setting as the coupling scoring function. Multiple sequence alignment was done with default settings and resulted in 468 sequences with a e-value cut off of −3. The top 50 amino acid residues (see Table S3) that showed evolutionary coupling to AtSLAC1-V272 and V273 were highlighted on previously generated homology models [36] using VMD [37].

Frequency logos of TMD1 to 3

Selected SLAC1 homologs were identified by BLASTP (Sequences can be found in Table S4). Sequences were aligned using MUSCLE [52] with a gap open penalty of −2.9, gap extend of 0 and hydrophobicity multiplier of 5. Transmembrane helix 1, 2 and 3 were identified in the homology model of AtSLAC1 [18] using chimera [54]. Frequency logos were created based on alignments of transmembrane helix 1, 2 and 3 using the weblogo program [53]. Jalview [55] was used to visualize transmembrane helix 1, 2 and 3 alignments.

Alignment, phylogenetic analysis and inference of ancestral SLAC1

Alignment

Selected SLAC1 homologs were identified by BLASTP. Sequences were aligned using MUSCLE [52] with a gap open penalty of −2.9, gap extend of 0 and hydrophobicity multiplier of 5. Gaps introduced by parts of the sequence supported by 4 or less genes were trimmed.

Phylogenetic analysis

MrBayes 3.2.6 [56] was used to infer the Bayesian phylogenetic tree as previously described [66]. Briefly, Prottest v3.4.2 [57] identified the appropriate LG based phylogenetic model as LG+I+G that use a general amino acid replacement matrix [67] with a proportion of invariable sites (+I) [68] that use a gamma distribution for modeling the rate heterogeneity (+G) [69]. Bayesian inference trees were calculated until convergence was reached ("average standard deviation of split frequencies" < 0.01). The temperature heating parameter was set to 0.05 (temp = 0.05) to increase the chain swap acceptance rates, this reduce the chance of Markov chains getting stuck at local high-probability peaks. Burn-in was set to 25% (burninfrac = 0.25) and the number of Markov chains was set to 8 (nchains = 8).

RAxML

The maximum likelihood phylogenetic tree was inferred using RAxML 8.2.9 as previously described [66]. Briefly, Prottest v3.4.2 [57] identified LG+I+G as the best phylogenetic model. 1000 bootstrap replicate searches were performed, and the bootstrap values were portrayed on the MrBayes generated consensus tree when MrBayes values were below 0.95. SLAC1 from *MP* was used as the out-group. All analyses were run in MPI via the CIPRES SCIENCE GATEWAY [70] at the San Diego Supercomputer Center (SDSC). Trees were visualized in figtree (http://tree.bio.ed.ac.uk/software/figtree/) and annotated with Adobe Illustrator.

Inference of ancestral sequence

The topology of the phylogenetic tree inferred by MrBayes and RAxML were identical and we used this multiple sequence alignment and the phylogenetic tree as input for inference of the ancestral sequence of the last common ancestor of monocots and dicots. Probabilities for the ancestral sequence at the split between monocots and dicots (Figure S4A) was calculated using the LG model of substitution by FastML [43]. The top 100 most likely sequences showed a log likelihood difference of only 0.19 which suggests that sequence #1 and #100 are almost as likely to be true. The N- and C terminus of SLAC1 has activating/regulatory roles and thus we, respectively, substituted the residues 1-182 and 514-556 from the AncSLAC1 N- and C-terminal residues with the corresponding residues from AtSLAC1 (for sequence information see Table S4). We resurrected AncSLAC1 by GeneStrand synthesis (Eurofins Medigenomix GmbH, Campus Ebersberg, Germany).

QUANTIFICATION AND STATISTICAL ANALYSES

All experiment was performed at least two times (independent experiments). Sample size, n, and statistical details (mean ± standard error, SE or standard deviation, SD) for each experiment are given in the figure legends. Statistical significances based on one-way ANOVA. For statistical analysis the software Igor Pro7 (waveMetrics, Inc., Lake Oswego, Oregon, USA), Excel (Microsoft Corp. Redmond, Washington, USA) was used.

DATA AND SOFTWARE AVAILABILITY

The accession number for the raw RNA-seq sequence reads reported in this paper is ArrayExpress: E-MTAB-5877.

Accession numbers

HvSLAC1 (*Hordeum vulgare* cultivar Barke); AtSLAC1 (*Arabidopsis thaliana* Col-0) At1g12480; OsSLAC1 (*Oryza sativa* Japonica Group) XP_015636891; SlSLAC1 (*Solanum lycopersicum*) XP_004245686; NtSLAC1 (*Nicotiana tabacum*) XP_016515379; ZomSLAC1 (*Zostera marina*) KMZ58505; PdSLAC1 (*Phoenix dactylifera*) XP_008780343.1; PpSLAC1 (*Physcomitrella patens*) PNR63146.1; CrSLAC1a (*Ceratopteris richardii*) KT238910; SmSLAC1b (*Selaginella moellendorffii*) KU556809; AtOST1 (*Arabidopsis thaliana* Col-0) At4g33950; AtCPK6 (*Arabidopsis thaliana* Col-0) At2g17290; AtABI1 (*Arabidopsis thaliana* Col-0) At4g26080.

Software and algorithms used in this study are listed in the Key Resources Table. In addition, for graph preparations and statistical analysis the software Igor Pro7 (waveMetrics, Inc., Lake Oswego, Oregon, USA), Excel (Microsoft Corp. Redmond, Washington, USA), Adobe Illustrator (Adobe Systems Incorporated, San Jose, California, USA) and CorelDRAW (Corel Corporation, Ottawa, Ontario, Canada) was used.